



**Acoustics'08  
Paris**  
June 29-July 4, 2008  
[www.acoustics08-paris.org](http://www.acoustics08-paris.org)

## A GWBEM method for high frequency acoustic scattering

Emmanuel Perrey-Debain, Hadrien Bériot, Mabrouk Ben Tahar and Catherine Vayssade

Université de Technologie de Compiègne, Lab. Roberval UMR 6253, Dept. Acoustique, BP 60319, 60203 Compiègne, France  
emmanuel.perrey-debain@utc.fr

This paper considers the problem of scattering of a time-harmonic acoustic incident wave by a hard obstacle. The numerical solution to this problem is found using a GalerkinWave Boundary Element Method (GWBEM) whereby the functional space is built as the product of conventional low order piecewise polynomials with a set of plane waves propagating in various directions. In this work we present strategies for finding the appropriate plane wave basis locally on each boundary element in order to deal efficiently with very irregularly meshed structures exhibiting both large smooth scattering surfaces as well as corners and small geometrical features. Numerical results clearly demonstrate that these improvements allow the handling of scatterers with complicated geometries while maintaining a low discretization level of 2.5 to 3 degrees of freedom per full wavelength.

## 1 Introduction

It is well known that the use of discrete (frequency domain) numerical methods for the solution of the Helmholtz equation is limited to problems in which the wavelength under consideration is not small in comparison with the domain size. The limitation arises because conventional elements, based on polynomial shape functions require around ten variables per full wavelength. Following earlier predictions of de La Bourdonnaye [1], it has been found that drastic progress can be made by including a plane wave basis in a collocation boundary element formulation. This gave rise to the so-called ‘wave boundary elements’(WBE) capable of containing many oscillations [2, 3]. In practical terms, the results of this work showed that, for any given amount of computational resource, these WBE enable the supported frequency range to be extended by a factor of 3 to 4 over conventional boundary elements for two-dimensional cases. Though these developments proved to be very successful, all the studies previously published involved the use of a *constant* number of plane wave directions on regularly meshed and analytically described smooth scatterers. Furthermore, the method’s performances depend on the number and locations of the collocation points [3] and this is particularly relevant for tridimensional obstacles for which the number of points must largely exceed the number of variables [4]. This yields overdetermined systems that require the use of adequate solvers. Because of these limitations, the work carried out so far only represent the early developments in a new BEM approach. In the present paper, we go one step further by tackling more realistic engineering geometries. Our aim is mainly to propose new strategies for finding the appropriate plane wave basis locally on each WBE in order to deal efficiently with very *irregularly* meshed structures exhibiting both large smooth scattering surfaces as well as corners and small geometrical features. This paper will show that these improvements allow the handling of scatterers with complicated geometries while maintaining a low global discretization level of 2.5 to 3 degrees of freedom per wavelength.

## 2 Problem statement

We consider the scattering of an time-harmonic acoustic incident wave  $\phi^i$  by a bounded obstacle  $\Omega'$  in a bidimensional homogeneous propagative medium  $\Omega$  of characteristic sound speed  $c_0$ . Let  $\kappa = \omega/c_0$  denote the associated wavenumber; we aim at finding the scattered wave field

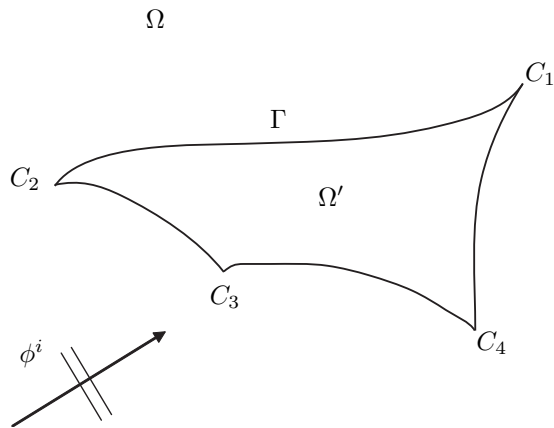


Figure 1: The model scattering problem.

$\phi^s$  satisfying ( $e^{-i\omega t}$  time-dependence)

$$\Delta\phi^s + \kappa^2\phi^s = 0 \quad \text{in } \Omega, \quad (1)$$

as well as the usual radiation condition,

$$\lim_{|x| \rightarrow \infty} \sqrt{|x|} \left( \frac{\partial\phi^s}{\partial|x|} - i\kappa\phi^s \right) = 0. \quad (2)$$

In this work, we shall consider Neumann type conditions on the surface of the scatterer  $\Gamma = \partial\Omega'$ , i.e., the total field  $\phi = \phi^i + \phi^s$  must satisfy

$$\frac{\partial\phi}{\partial n}(x) = \nu(x), \quad x \in \Gamma. \quad (3)$$

Using a direct combined integral representation, the unknown field  $\phi(x)$  on  $\Gamma$  is found to be the unique solution of the second kind integral equation [5]

$$L\phi = \left( \frac{1}{2} + D + \alpha H \right) \phi = g \quad \text{on } \Gamma \setminus \{\mathcal{C}\} \quad (4)$$

where  $\{\mathcal{C}\}$  is the set of corners of  $\Omega'$  and  $g$  stems for the incident field and the radiation term  $\nu$ ,

$$g = \phi^i + \alpha \frac{\partial\phi^i}{\partial n} + \left( S + \alpha D^* - \frac{\alpha}{2} \right) \nu \quad (5)$$

and  $S, D, D^*$  and  $H$  stand respectively for the usual single layer potential operator

$$S\phi(x) = \int_{\Gamma} G(x, y)\phi(y)d\gamma_y, \quad (6)$$

the double layer potential operator

$$D\phi(x) = \int_{\Gamma} \frac{\partial G(x, y)}{\partial n_y} \phi(y)d\gamma_y, \quad (7)$$

its adjoint operator

$$D^* \phi(x) = \frac{\partial}{\partial n_x} \int_{\Gamma} G(x, y) \phi(y) d\gamma_y, \quad (8)$$

and the hypersingular operator

$$H\phi(x) = \frac{\partial}{\partial n_x} \int_{\Gamma} \frac{\partial G(x, y)}{\partial n_y} \phi(y) d\gamma_y. \quad (9)$$

The kernel  $G$  stands for the free-space Green function  $G(x, y) = i/4H_0^1(\kappa|x - y|)$  and  $n_y$  (resp.  $n_x$ ) is the inward normal unit vector at point  $y$  (resp.  $x$ ).  $H_0^1$  denotes the Hankel function of the first kind of zero order. The coupling coefficient  $\alpha$  must have a non-zero imaginary part to ensure the uniqueness of the solution. As we are not dealing with very low frequency applications, we shall take  $\alpha = i/\kappa$ .

## 3 GWBEM formulation

### 3.1 Standard $p$ -formulation

In the Galerkin method, we convert the original equation (4) into an equivalent variational formulation, i.e. we consider the following problem (symbol \* denotes the complex conjugate):

$$\text{Find } \phi \in \mathcal{V} \text{ such that} \\ (\varphi^*, \mathcal{L}\phi)_{\Gamma} = (\varphi^*, g)_{\Gamma}, \quad \forall \varphi \in \mathcal{V}, \quad (10)$$

where  $\mathcal{V}$  is an appropriate functional space ( $\mathcal{V} = H^{1/2}(\Gamma)$  in this case) and  $(\cdot, \cdot)_{\Gamma}$  denotes the usual scalar product on  $\Gamma$ . Following standard procedure [6], Eq (10) may be integrated numerically by subdividing the boundary into elements, over each of which the potential may be expressed in terms of nodal values according to conventional interpolation using Lagrangian shape functions, i.e.

$$\phi = \mathbf{N}^T \mathbf{a}, \quad (11)$$

where  $\mathbf{N}$  is a vector containing the shape functions and  $\mathbf{a}$  is a vector containing the nodal potentials. The superscript  $T$  denotes transpose of a matrix or vector. Although this approach is usually implemented using low-order polynomials (linear or quadratic), high-order basis function are considered in this work in order to give a fair comparison with the plane wave based approach. In all cases, evenly spaced nodes in the parametric space  $\eta \in [-1, 1]$  are used and  $p$ -order Lagrangian shape functions take the generic form

$$N_q^p(\eta) = \prod_{r=1, r \neq q}^{p+1} \frac{\eta - \eta_r}{\eta_q - \eta_r} \quad \text{for } q = 1, \dots, p+1, \quad (12)$$

where  $\eta_r = 2(r-1)/p-1$  corresponds to the node location.

### 3.2 Plane waves formulation

The wave boundary element discretization of (10) starts with the introduction of a set of  $J$  nodes located on  $\Gamma$ ,

$$\mathcal{N} = \{x_j \in \Gamma, j = 1, \dots, J\}. \quad (13)$$

These points must coincide with the corners of  $\Omega'$  so that  $\mathcal{C} \subset \mathcal{N}$ . We assume that the geometry of the scatterer  $\Gamma_j$  between two consecutive nodes  $x_j$  and  $x_{j+1}$  is known analytically, or can be simulated by appropriate approximation methods (via Lagrange interpolation for instance), i.e. there exists a regular function  $\gamma_j$  defined on the reference interval  $[-1, 1]$  such that

$$\Gamma_j = \{\gamma_j(\eta), \eta \in [-1, 1]\}, \quad (14)$$

with the convention that  $x_j = \gamma_j(-1)$ ,  $x_{j+1} = \gamma_j(1)$  and  $x_{J+1} = x_1$ . We introduce a set of  $M_j$  plane wave directions ‘attached’ to each node  $x_j$ . In this work, these direction are chosen to be regularly distributed as

$$\zeta_j^m = \begin{pmatrix} \cos(m2\pi/M_j + \delta\theta_j) \\ \sin(m2\pi/M_j + \delta\theta_j) \end{pmatrix}, \quad (15)$$

where  $m = 1, \dots, M_j$  and  $\delta\theta_j$  defines the angular origin of the wave basis directions. On each element  $\Gamma_j$ , the potential  $\phi$  is approximated as the following plane wave expansion

$$\phi(x) = P_j^0(x) \mathbf{w}_j^T(x) \mathbf{A}_j + P_j^1(x) \mathbf{w}_{j+1}^T(x) \mathbf{A}_{j+1}. \quad (16)$$

The vector function  $\mathbf{w}_j(x)$  denotes the set of plane wave

$$\mathbf{w}_j^T(x) = \langle w_j^1(x), \dots, w_j^{M_j}(x) \rangle, \quad (17)$$

where  $w_j^m(x) = \exp[i\kappa \zeta_j^m \cdot (x - x_j)]$  is a propagative plane wave traveling in the  $\zeta_j^m$ -direction. The unknown coefficients  $\mathbf{A}_j = \langle A_j^1, \dots, A_j^{M_j} \rangle^T$  can be interpreted as the amplitudes of the associated plane waves. Functions  $P_j^0$  and  $P_j^1$  must be sufficiently regular and chosen as to ensure continuity of the potential on the boundary of the scatterer. This condition is met by requiring that

$$P_j^0(x_j) = P_j^1(x_{j+1}) = 1, \quad P_j^0(x_{j+1}) = P_j^1(x_j) = 0, \quad (18)$$

so that at each node  $x_j$ , the potential is only dependent on  $\mathbf{A}_j$  and can be easily recovered as  $\phi(x_j) = \mathbf{e}^T \mathbf{A}_j$  where  $\mathbf{e}^T = \langle 1, \dots, 1 \rangle$ . In order to satisfy the continuity condition (18), it suffices to take

$$P_j^0(x) = N_2^1(\eta) \quad \text{and} \quad P_j^1(x) = N_1^1(\eta), \quad (19)$$

where the correspondence between the point  $x$  located on  $\Gamma_j$  and the parameter  $\eta$  is naturally given by  $x = \gamma_j(\eta)$ . Shape functions  $N_1^1, N_2^1$  form the linear Lagrangian basis which explicit form is given in Eq (12). For the sake of illustration, the top of Fig 2 shows a typical piecewise polynomial discretization for the acoustic potential on the boundary line with 5 boundary elements. On the bottom, the potential is expanded in the plane wave basis which directions are ‘attached’ to the nodes located at the extremity of the boundary line. For a brief nomenclature, such a boundary element on which the wave field is described by the plane wave expansion (16) will be referred to as a 2-node WBE. Applying the standard Galerkin weighting procedure, the weighting functions are expanded in terms of the same set of wave functions used in the expansion (16). This yields the matrix system

$$\mathbf{L}_w \mathbf{A} = \mathbf{g}_w, \quad (20)$$

where  $\mathbf{A} = \langle \mathbf{A}_1^T, \dots, \mathbf{A}_J^T \rangle^T$  contains the amplitudes of the plane waves basis functions. Here, we introduce the

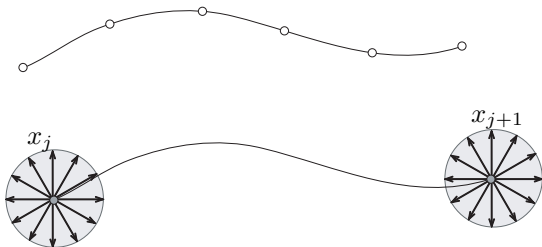


Figure 2: Discretization of the potential on the boundary line. Top: Classical piecewise polynomials approximation with 5 boundary elements; Bottom: The plane wave basis expansion on a 2-node WBE.

subscript  $w$  as a reference to the plane wave boundary element formulation. The total number of degrees of freedom is simply given by  $N_w = \sum_{j=1}^J M_j$ . In the 2-node wave boundary element formulation just described, one can note that the set of unknown amplitudes  $A_j$  at node  $x_j$  have contribution on the two adjacent wave boundary elements  $\Gamma_{j-1}$  and  $\Gamma_j$ , thus the plane waves enrichment can not be done locally on a single element. This point has practical consequences when dealing with irregular meshes and we will comment on this further.

## 4 A Benchmark problem

In this section, some results for the scattering of an incident plane wave  $\phi^i(x) = \exp(i\kappa d \cdot x)$  propagating along the horizontal direction  $d = (1, 0)$  by a hard circular cylinder of radius  $a$  are presented. In polar co-ordinates, the field can be represented by separable solutions and the exact scattered potential  $\tilde{\phi}^s$  on the boundary is given by the infinite series:

$$\tilde{\phi}^s(x) = - \sum_{n=0}^{\infty} (1 + \delta_{0,n}) i^n \frac{J'_n(\kappa a) H_n(\kappa a)}{H'_n(\kappa a)} \cos(n\theta), \quad (21)$$

where  $x = a(\cos \theta, \sin \theta)$  and  $\delta$  is the usual Kronecker symbol. Functions  $H_n$  and  $J_n$  are respectively, Hankel and Bessel functions of the first kind and order  $n$ , and primes denotes differentiation with respect to their arguments. This series is well behaved and allows one to produce very accurate results without deterioration at high frequency. By using the Bessel's first integral identity [7], the trigonometric term  $\cos(n\theta)$  in (21) admits a plane wave integral representation which, after discretization, can be approximated up to any desired accuracy as a finite plane waves series. This result can be generalized to any pointwise convergent Fourier series with respect to the azimuthal angle  $\theta$  [8]. In this context, the plane wave basis expansions (16) is expected to produce very accurate results. These can be conveniently displayed by plotting the overall  $L^2$  error (in percent)

$$E_2(\%) = 100 \times \frac{\|\phi - \tilde{\phi}\|_{L^2(\Gamma)}}{\|\tilde{\phi}\|_{L^2(\Gamma)}} \quad (22)$$

against the *global* discretization level  $\tau$  defined as

$$\tau = \frac{\lambda N_{dof}}{\text{ar}(\Gamma)}, \quad (23)$$

where  $\lambda$  is the wavelength,  $N_{dof}$  denotes the total number of degree of freedom and  $\text{ar}(\Gamma) = \int_{\Gamma} d\gamma(x)$  stands for the perimeter of  $\Gamma$ . In equation (22), functions  $\phi$  and  $\tilde{\phi}$  denote the computed and exact total wave field on the surface of the scatterer respectively. The effi-

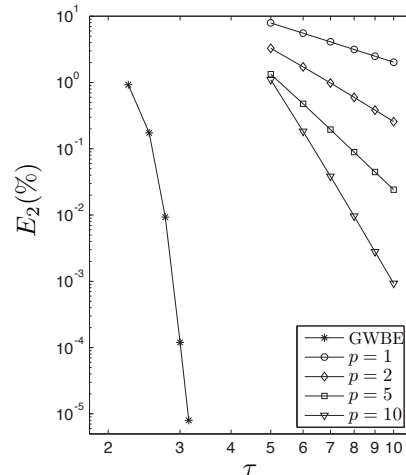


Figure 3: Convergence rates for the case of the plane wave scattering by a rigid cylinder,  $\kappa a = 100$ .

ciency of the plane wave basis is clearly confirmed in Fig 3 showing a comparison of the convergence rate of the 2-node plane wave based approximation (16) (referred to as the Galerkin Wave Boundary Element or GWBE) using  $J = 4$  wave boundary elements with  $M$  planes waves attached to each node and the standard  $p$ -order Lagrangian interpolation. The evolution of the GWBE error as  $\tau$  increases (note that the associated number of wave directions  $M$  is recovered by inverting (23)) shows superconvergence rates and these results are comparable with some theoretical predictions (see Fig.2 in [8]). It is now well known that the 'price' to pay for such remarkable accuracy is manifested in matrices with very high condition number. In these severe scenarios, it was found beneficial to discard very small singular values likely to be corrupted by round-off errors. In the following examples, all computations are carried out using such a truncation whenever the condition number (in the 2-norm) exceeds  $10^{12}$ . In the other cases, there is no filtering and the matrix system is inverted using standard algebraic solvers. In [2], it was numerically observed that the plane waves approximation yields better results at high frequency and this is in agreement with earlier predictions based on geometrical optics arguments. In practice and for a given geometry, the question arises as to what 'high frequency' means. To cope with this issue, we found it relevant to consider the *local* reduced wave number  $\beta_j$  defined as the number of wavelengths spanned by the WBE  $\Gamma_j$ :

$$\beta_j = \frac{h_j}{\lambda}, \quad (24)$$

where  $h_j$  is the length of  $\Gamma_j$ . To simplify the analysis, the circular scatterer is first regularly meshed using

$J = 10$  WBE. In this case, all the  $\beta_j$ 's are equal to the same value (let us call it  $\beta$ ). The method's performances are conveniently highlighted by studying the evolution of the overall error  $E_2$  with respect to the discretization level  $\tau$  and the number of oscillations  $\beta$  contained within a wave boundary element. Through intensive calcula-

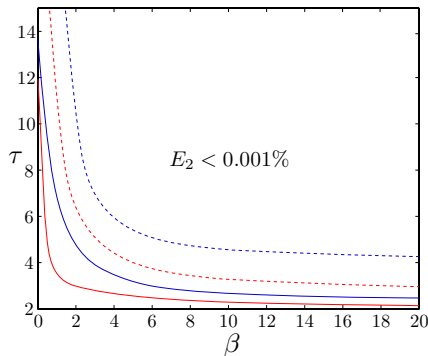


Figure 4: Scattering by a rigid circular cylinder regularly meshed with  $J = 10$  WBE (red color) and  $J = 2$  WBE (blue color).  $L^2$  error isolines,  $E_2 = 1\%$  (solid line) and  $E_2 = 0.001\%$  (dashed line)

tions, such dependence has been investigated over a fine grid on the rectangular domain  $(\beta, \tau) \in [0, 20] \times [2, 15]$ . In Fig 4 (are plotted, in red color, the isolines of the quadratic error. The blue color isolines correspond to the same study by using only  $J = 2$  WBE. All these results display a L-curve pattern which characterizes what we may interpret as the plane wave approximation trade-off. The upper right area above the last isoline can be identified as the over-discretization region where very high accuracy can be obtained at the price of very ill-conditioned matrices. If best results (in terms of reducing the complexity) are obtained when using large elements (say  $\beta > 5$ ), the associated system matrices are likely to be nearly ill-conditioned and the use of the SVD solver might be necessary. Ill conditioning effects can also be met when small elements are over-discretized. Using curve fitting algorithms, it is possible to extract an approximation of the  $E_2$  isolines. Here, we propose the following empirical law

$$\tau \approx \frac{C}{\beta^{0.8}} + 2, \quad (25)$$

where  $C$  is a constant which depends on the expected level of precision, given in Table 1. The differences between the cases  $J = 10$  and  $J = 2$  highlight the fact that the geometric distortion also has an influence on the precision of the method and straight elements show better performance than curved ones. The asymptotic behaviour that  $\tau \rightarrow 2$  when  $\beta \rightarrow \infty$  is consistent with [2, 4] and share some similarities with the well known sampling theorem. All these developments will be helpful in the remainder.

$E_2$	$J = 10$	$J = 2$
1%	$C = 2$	$C = 4$
0.001%	$C = 8$	$C = 12$

Table 1: Determination of constant  $C$ .

## 5 Numerical examples

This section addresses the major issue on the ability of the wave based method to handle irregular meshes with patches of varying sizes. For this purpose the test geometry given in Fig 5 has been considered. It represents a non-convex scatterer with sharp corners, consisting of a square of size  $a$  exhibiting a small cavity of characteristic length  $b$ . The boundary is discretized using 8 WBE

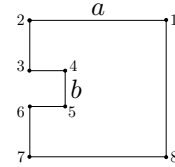


Figure 5: Square with a cavity.

and the associated nodes are numbered ranging from 1 to 8 as shown. Thus, the mesh comprises three different element sizes:  $h_1 = a$ ,  $h_2 = a - b$  and  $h_3 = b$ . For a given frequency, the problem naturally arises as to guess the right number of plane waves at the nodes. To illustrate the strategy, we consider a cavity of size  $b = a/10$  at  $\kappa a = 100$ . For a given accuracy, the required discretization level on each WBE is given by applying the isoline approximation formula (25) locally as a function of the number of oscillations spanned by the element  $\Gamma_j$ , i.e., we take

$$\tau_j = \frac{C}{\beta_j^{0.8}} + 2, \quad (26)$$

where  $\tau_j$  now stands for the *local* discretization level. Let us consider, for instance, an expected precision of about 1%; since the elements have no geometric distortion we shall take  $C = 2$  as suggested in Table 1. We give in Table 2 the repartition of  $\tau_j$  for the first three wave boundary elements.

	$j = 1$	$j = 2$	$j = 3$
$h_j$	1	0.45	0.1
$\beta_j$	$50/\pi$	$22.5/\pi$	$5/\pi$
$\tau_j$	2.22	2.41	3.38

Table 2: Local discretization levels at  $\kappa a = 100$ , with  $b = a/10$  for an expected precision of 1% ( $C = 2$ ).

As mentioned earlier, the 2-node WBE formulation has the drawback that each set of plane waves contribute to approximate the wave field on two consecutive elements. Thus, there is no simple correspondence between the local discretization level and the number of plane waves except for regularly meshed geometries. To overcome this difficulty, we define  $\tau_j$  as the average number of plane waves contributing in approximating the wave field on the element  $\Gamma_j$ , this gives

$$\tau_j = \frac{\lambda(M_j + M_{j+1})}{2h_j}. \quad (27)$$

With this definition, it is clear that the homogeneous case  $M_j = M_{j+1}$  is recovered. Now, inverting equation (27) for all  $j = 1, \dots, J$  yields the following linear system:

$$\text{QM} = \text{L}, \quad (28)$$

where the vector  $(L)_j = 2\beta_j\tau_j$  contains the number of variables required per element and  $M = \langle M_1, \dots, M_J \rangle^T$ . The connectivity matrix  $Q$  has the property of being always singular when  $J$  is even and  $\det Q = 2$  when the number of elements is odd. Note however that the invertibility of matrix  $Q$  does not guarantee a ‘good’ solution  $M$  as it may happen that some of the  $M_j$ ’s have negative values. Thus, system (28) can not be solved in the usual manner. To alleviate these difficulties, we introduce the residual vector

$$R = QM - L, \quad (29)$$

and we look for a quasi-optimal solution vector  $M_{opt}^T$  as to minimize the fitness function

$$F(M) = \|R\|_2 + \rho \sum_{j=1}^J (\min(0, R_j))^2, \quad (30)$$

where  $R_j = (R)_j$  and the penalty term in the right hand side is added to ensure that the discretization constraint (27) is satisfied everywhere along the boundary. As the function  $F(M)$  is likely to contain a large number of local minima, a global optimization strategy was necessary. In this work, we have chosen to develop and apply an evolutionary algorithm [9]. In Fig 6, performances of the strategy are compared with those obtained using a more naive approach in which the number of plane waves  $M$  is taken constant at all nodes. Standard BEM results ( $p = 2$ ) are also shown in order to give a fair comparison with conventional discretization techniques. Here, the test case is an artificial radiating problem for which an exact analytical solution is available. All calculations except the BEM ones have been carried out by simply choosing different values for the constant  $C$  in (25). In order to validate the method on a scattering problem. We consider the same obstacle with a cavity of size  $b = a/20$ , impinged by a plane wave of incidence  $\theta^i = \pi/4$  at the frequency  $\kappa a = 68$ . There is no analytical solution for this problem and the GWBE solution is compared with a reference solution computed with standard quadratic BEM on a very refined mesh. Fig. 7 shows the real part of the total acoustic field in the propagative medium surrounding the scatterer showing the effect of the cavity in the scattering pattern.

## References

[1] de La Bourdonnaye A. A microlocal discretization method and its utilization for a scattering problem. *C. R. A. S. Paris. Série I* 1994; **318**:385–388.

[2] Perrey-Debain E, Trevelyan J, Bettess P. Plane wave interpolation in direct collocation boundary element method for radiation and wave scattering: numerical aspects and applications. *J. Sound Vib.* 2003; **261**(5):839–858.

[3] Perrey-Debain E, Trevelyan J, Bettess P. Use of wave boundary elements for acoustic computations. *J. Comp. Acou.* 2003; **11**(2):305–321.

[4] Perrey-Debain E, Laghrouche O, Trevelyan J, Bettess P. Plane wave basis finite elements and boundary elements for three dimensional wave scattering.

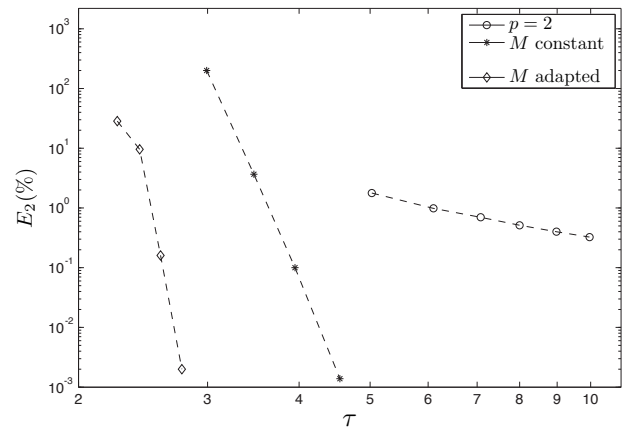


Figure 6: Convergence rates for the radiating square shape with a small feature of size  $b = a/10$  at  $\kappa a = 100$ .

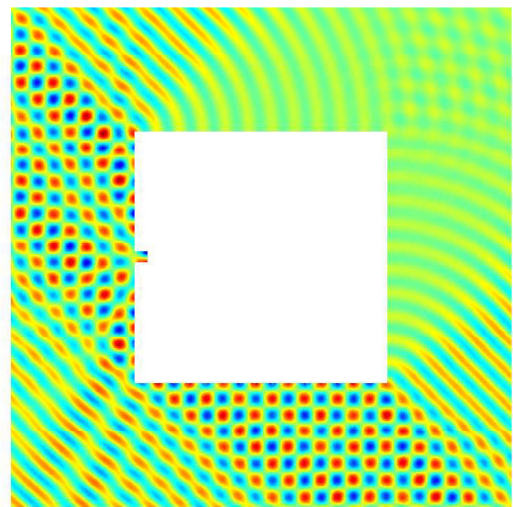


Figure 7: Total field (real part) around the scatterer at  $\kappa a = 68$  for a plane wave of incidence  $\theta^i = \pi/4$ .

*Phil. Trans. Roy. Soc. London A* 2004; **362**:561–577.

[5] Burton AJ, Miller GF. The application of integral equation methods to the numerical solution of some exterior boundary-value problems. *Phil. Trans. Roy. Soc. London A* 1971; **323**:201–210.

[6] Ciskowski RD, Brebbia CA. *Boundary Element Methods in Acoustics*. Computational Mechanics Publications, Southampton, 1991.

[7] Abramowitz M, Stegun IA. *Handbook of Mathematical Functions*, 10th Edition, Applicable Mathematics Series, Vol. 55, National Bureau of Standards, US Government Printing Office, Washington, DC, 1972.

[8] Perrey-Debain E. Plane wave decomposition in the unit disc: convergence estimates and computational aspects. *J. Comp. Appl. Math.* 2006; **193**:140–156.

[9] Michalewicz Z. *Genetic Algorithms + Data Structures = Evolution Programs*. Springer-Verlag, Berlin, 1996.